

Study of Edge Transport Barrier Formation on CHS Plasma

Takashi MINAMI, Shoichi OKAMURA, Tsuyoshi AKIYAMA, Mitsutaka ISOBE, Tetsutaro OHISHI¹⁾, Haruhisa NAKANO²⁾, Katsumi IDA, Akihide FUJISAWA, Kiichiro NAKAMURA, Kenichi NAGAOKA, Mikiro YOSHINUMA, Chihiro SUZUKI, Yasuo YOSHIMURA, Kazuo TOI, Masaki NISHIURA, Shinsuke OHSHIMA³⁾, Zenzo NARUHIRO, Harukazu IGUCHI, Shin NISHIMURA, Akihiro SHIMIZU, Keisuke MATSUOKA and Chihiro TAKAHASHI

National Institute for Fusion Science, Toki 509-5292, Japan

¹⁾*Department of Quantum Engineering and System Science, Tokyo University, Tokyo 113-8656, Japan*

²⁾*Department of Fusion Science, The Graduate University for Advanced Studies, Toki 509-5292, Japan*

³⁾*Department of Energy Engineering and Science, Nagoya University, Nagoya 464-8603, Japan*

(Received 16 June 2005 / Accepted 20 April 2006)

An edge transport barrier (ETB) similar to the tokamak H-mode has been observed for beam-heated plasma with two co-injected Neutral Beam Injectors (NBIs) in CHS. The H_α emission showed a clear spontaneous drop followed by an increase of line-averaged electron density at the L-H transition. Stored energy increased by $\sim 40\%$ with H-factor improvement up to $\sim 30\%$ compared to the international stellarator scaling (ISS04v03). A rapid density increase in the edge region to two-times level of the L-mode was observed to accompany a $\sim 15\%$ increase in the density gradient. An ETB was formed when the plasma density exceeded the lower density limit by $\sim 1.5 \times 10^{13} \text{ cm}^{-3}$ and the total NBI power exceeds the threshold level ($P_{\text{deposit}}/\bar{n}_e \sim 200 \times 10^{-13} \text{ kW/cm}^{-3}$ at $B_T = 0.95 \text{ T}$, $R_{\text{ax}} = 92.1 \text{ cm}$, where P_{deposit} is the deposited NBI power, \bar{n}_e is electron density, B_T is toroidal magnetic field strength and R_{ax} is location of magnetic axis). The power threshold increased with the magnetic field strength, as in tokamak scaling, and depends on the magnetic field configuration of the helical plasma.

© 2006 The Japan Society of Plasma Science and Nuclear Fusion Research

Keywords: edge transport barrier, helical plasma, H-mode, plasma confinement, improved confinement, threshold power, H-mode scaling, CHS

DOI: 10.1585/pfr.1.032

1. Introduction

The formation of transport barriers to enhance L-mode confinement is important for helical plasma as well as tokamak plasma. Investigating the structure of the improved confinement region and comparing the formation conditions for various transport barriers (e.g. edge, internal on tokamak and helical plasmas) is essential to understanding the physical mechanism of the barrier formation.

There are two kinds of transport barriers: internal transport barriers and edge transport barriers. Both types of transport barriers have been observed in the compact helical system (CHS). The internal transport barrier of CHS is formed for low-density plasma with electron cyclotron heating (ECH). A sharp gradient is created on the electron temperature profile at the barrier location. The magnitude of density fluctuation is clearly reduced at locations of steep electron temperature gradient from large radial electric field shear [1, 2]. The electric field shear is created by a large positive electric field due to the electron root existence in the plasma core region, which is produced by the high electron temperature from ECH. The electric field is determined by the ambipolar diffusion of neoclas-

sical particle fluxes; hence we call this ITB a neoclassical internal transport barrier (N-ITB) [1, 3]. Energy confinement improvement for both ions and electrons has been confirmed for N-ITB plasma. However, the effect on the particle transport is not clear because the density profile is not changed by the N-ITB transition. There is an upper density limit ($< 6 \times 10^{12} \text{ cm}^{-3}$) and a threshold power ($P_{\text{ECH}} > 150 \text{ kW}$) for the N-ITB formation. These thresholds values are explained by the conditions for realizing the electron root in the core region. In order to obtain high-performance plasma, it is important to increase the upper density limit and to expand the electron root region in the N-ITB plasma.

Another transport barrier of helical plasma such as the tokamak H-mode is the edge transport barrier (ETB). ETBs were found around the same time in CHS and W7-AS devices [4–6]. An ETB can be created for high-density plasma ($> 1.5 \times 10^{13} \text{ cm}^{-3}$ on CHS), and is favorable for achieving a good plasma performance. In previous CHS experiments (1992), the ETB could be created by controlling the rotational transform in the plasma edge region with an ohmic current generated by the ramp-up of the poloidal coil current [4, 5]. An ETB without net toroidal current

author's e-mail: minami@nifs.ac.jp

has been found by EC heating in the W7-AS Stellarator [6], and recently, a high-density ($2 \times 10^{14} \text{ cm}^{-3}$) H-mode (HDH) has been observed with an island divertor under NB heating and electron Bernstein wave heating [7]. These results expand the high-density operation regime of the helical plasma to the reactor regime. In an LHD experiment, the L-H transition with H_α emission drop was observed for plasma with a relatively high value ($\sim 1.5\%$) of average volume β (ratio of plasma pressure to magnetic field) [8]. On the heliotron J device, a spontaneous confinement transition like the ETB phenomena has been observed [9]. There are lower density limits for the barrier formation on these experiments; however, the existence of a power threshold as found in the tokamak experiments is not clear.

After two neutral beam injectors (NBIs) were modified from a blanced injection to two co-injections, the deposited NBI power increased; the ETB in the new operation regime was observed for NBI plasma without the ohmic current under a limiter configuration [10, 11]. The electron density in the outer region of the plasma considerably increased the formation of the new ETB and was thus being favorable for improving particle confinement. The key characteristics for the formation of this ETB are the lower density limit and the existence of an NB power threshold.

In this paper, first we report the time trace of global parameters of the new ETB plasma. Second, we discuss the changes in the density and temperature profiles before and after the L-H transition. Third, we discuss the ETB power threshold with the lower density limit for the L-H transition. Finally, the conclusion is presented.

2. Experimental Set-Up, Operation, and Global Behavior of Edge Transport Barrier

The CHS is a medium-sized heliotron-type device with a periodicity of $(l, m) = (2, 8)$. The major and averaged minor radii are 1.0 and 0.2 m, respectively. When the CHS is equipped with two co-NBIs (maximum power of each NBI is 0.8 MW) and two gyrotrons (53 GHz, 106 GHz), we can study plasma physical characteristics for a wide variety of input powers and heating methods.

Figure 1 shows time evolutions of H_α emissions with a visible spectrometer (a), a line-averaged density ($\rho = 0$ and $\rho = 0.63$, where ρ is normalized plasma minor radius) with the HCN interferometer (b), a stored energy with the diamagnetic loop (c), H-factor (d), a plasma current with the Rogowsky coil (e), and magnetic fluctuation with the magnetic probe (f). ETB discharge was performed under the magnetic field strength of 0.95 T and vacuum magnetic axis location of 92.1 cm, which corresponds to the standard magnetic configuration of a CHS. The target plasma was produced with ECH (electron cyclotron frequency $\omega_{\text{ech}}/(2\pi) \sim 53 \text{ GHz}$, injection power $P_{\text{inj}} \sim 200 \text{ kW}$), and

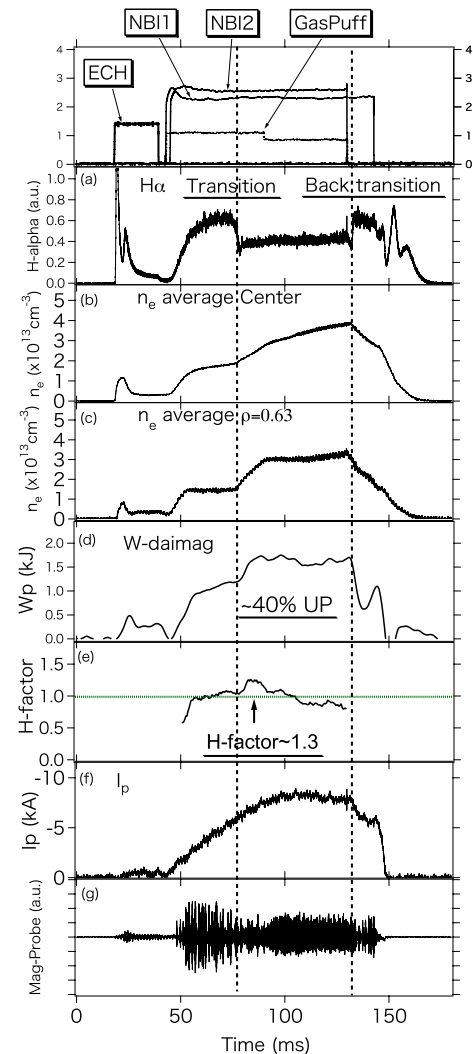


Fig. 1 Time evolution of ETB plasma. (a) H_α signal, (b) central line-averaged density, (c) line-averaged density at $\rho = 0.63$, (d) stored energy with diamagnetic measurement, (e) H-factor based on ISS04 scaling, (f) plasma current, (g) magnetic fluctuation.

the plasma was sustained by two co-NB injections. These NBIs have beam energies of $\sim 40 \text{ keV}$, $\sim 30 \text{ keV}$, respectively, and maximum port-through injected powers reach $\sim 800 \text{ kW}$, $\sim 700 \text{ kW}$, respectively (total power of two NBIs is $\sim 1,500 \text{ kW}$). When the heating power exceeded the power threshold and the line-averaged density exceeded the lower limit with gas-puffing ($\sim 1 \text{ MW}$, $1.5 \times 10^{13} \text{ cm}^{-3}$; details of the thresholds discussed later), the H_α signal showed a clear drop (at 75 ms). A clear back transition also exists $\sim 3 \text{ ms}$ after switch-off of the second NBI. The H_α drop was quick and spontaneous, which indicates the ETB phenomena has a transition nature similar to the N-ITB phenomena in CHS. An increase of the central line-averaged density following the transition was observed, as shown in Fig. 1 (b), and the line-averaged density of the outer chord ($\rho = 0.63$) simultaneously increased to the same level as the center chord, as shown in Fig. 1 (c), which

indicates that the shape of the density profile became hollow or flattened. The density of the outer chord was saturated ~ 20 ms after the transition, while the central chord kept increasing, so that the density increased and the profile shape changed from the flattened profile to the peaked profile 20 ms after the transition. A spontaneous H_α drop usually accompanies a peripheral density increase; therefore, it is a good indicator for the confirmation of the L-H transition.

The stored plasma energy obtained from the diamagnetic measurement also increased by $\sim 40\%$ from 1.2 kJ and was saturated during the ETB, although the density increased after the L-H transition. The stored energy ~ 5 ms after the transition corresponded to the H-factor value of ~ 1.3 (ISS04v04) [12]: a $\sim 30\%$ increase before the transition, as shown in Fig. 1 (e). The H-factor decreased ~ 20 ms after the transition because of the density dependence of the confinement scaling law. In usual NBI discharges on CHS, the H-factor value does not exceed the line that indicates H-factor equal to one. The plasma current increased constantly from the NBI injection (see Fig. 1 (f)). The current value of ~ 4 kA at the L-H transition induced a small change ($\Delta t \sim 0.02$, where t is rational transform) of an edge rotational transform in comparison to the ETB created by ohmic heating in the previous CHS experiments [4, 5]. The rational surface of $t = 1$ derived from the vacuum magnetic field calculation appeared around $\rho = 0.95$; however, a more accurate calculation taking into account the finite beta effect is required for the comparison between the last closed flux surface (LCFS) location and the rational surface. As shown in Fig. 1 (f), the magnitude of the magnetic oscillation increased ~ 20 ms after the transition, which resulted from the MHD activity ($m/n = 2/1(\omega/(2\pi)) \sim 4.5$ kHz), and $m/n = 1/1(\omega/(2\pi)) \sim 9$ kHz), which was caused by the steep pressure gradient from the formation of the transport barrier in the edge region.

3. Local Density and Temperature Profile Characteristics during ETB Transition

Local measurement for the electron density profile was performed with a multi-channel (24 channels) and high-repetition-rate (5 ms) YAG Thomson scattering system. Figure 2 (a) shows the experimental results for the ETB plasma when the magnetic strength was 0.95 T and the location of the magnetic axis was 92.1 cm. The open and closed circles denote the density profiles ~ 2 ms before and ~ 3 ms after the transition, respectively. The density profile changed from a peaked to a flattened shape just after the L-H transition, as shown in Fig. 2 (a). Figure 2 (c) shows the value of the density after the transition normalized by that before the transition. The density of the peripheral region ($\rho > 0.5$) just after the transition increased to approximately two times the density before the transi-

tion, which had a good quantitative agreement with the line-averaged density at $\rho = 0.63$ of the HCN measurement. Meanwhile, the increase of the core density was small.

In contrast, the change of the electron temperature in the edge region was not clear just after the transition. Figure 2 (b) shows the temperature before and after the transition; the two profiles are almost same in the whole plasma cross section. Figure 2 (e) shows the electron temperature after the transition normalized by the temperature before the transition. A symptomatic small increase in the electron temperature in $\rho > 0.8$ was observed just after the transition; after that, the edge temperature decreased due to the rapid increase of the edge electron density. We observed the temperature increase in the core region for several specific shots. The details are described in the next section.

The increase of the edge density suggests the buildup of the density gradient in the edge region ($\rho \sim 0.95$) resulting from the barrier formation. However, because the amount of the scattering light from the edge region ($\rho > 0.9$) was not adequate to measure the low electron temperature with a good S/N ratio, we performed a Li beam (15 kV) probe measurement, which is suitable for measuring the peripheral low-density plasma with high accuracy [13], as shown in the Fig. 3. The closed symbols denote the density profiles during the transition, and the open signals denote the profiles before the L-H transition and after the back transition. The YAG scattering measurement and the Li beam measurement are consistent as shown in Fig. 3 (a). Because the shape of the density profile before the transition is hollow as shown in Fig. 3 (a), the density increase of the edge region was approximately $\sim 30\%$ at $\rho \sim 0.9$. The density gradients increased by approximately 15% at $\rho \sim 0.8 - 0.95$ during the transition, and after the back transition the gradient rapidly fell to level observed before the transition. The electron density and the scale length of the density gradient ($L = n_e/(dn_e/dr)$) at $\rho \sim 0.9$ were changed from $L \sim -2.27$ cm, $n_e \sim 1.66 \times 10^{13}$ cm $^{-3}$ to $L \sim -2.30$ cm, $n_e \sim 2.23 \times 10^{13}$ cm $^{-3}$. These observations indicate that the barrier formation that enhances the reduction of the particle transport is around the $\rho \sim 0.95$. It was noted that in CHS experiments the shape of the density profile becomes almost always hollow or flattened by the ETB formation, while hollow, flattened and peaked profiles are observed before the transition. Consequently, the increase of the stored energy by $\sim 40\%$ at the ETB formation is mainly caused by the quick density increase in the plasma edge region resulting from the transport barrier formation.

The density transition times were further investigated with beam emission spectroscopy (BES), which measures the H_α emission from the interaction of the beam and the bulk electrons. BES has fast time resolution of 100 kHz and provides local information on the edge density [14]. BES signals both outside ($R = 107.5$ cm) and inside ($R =$

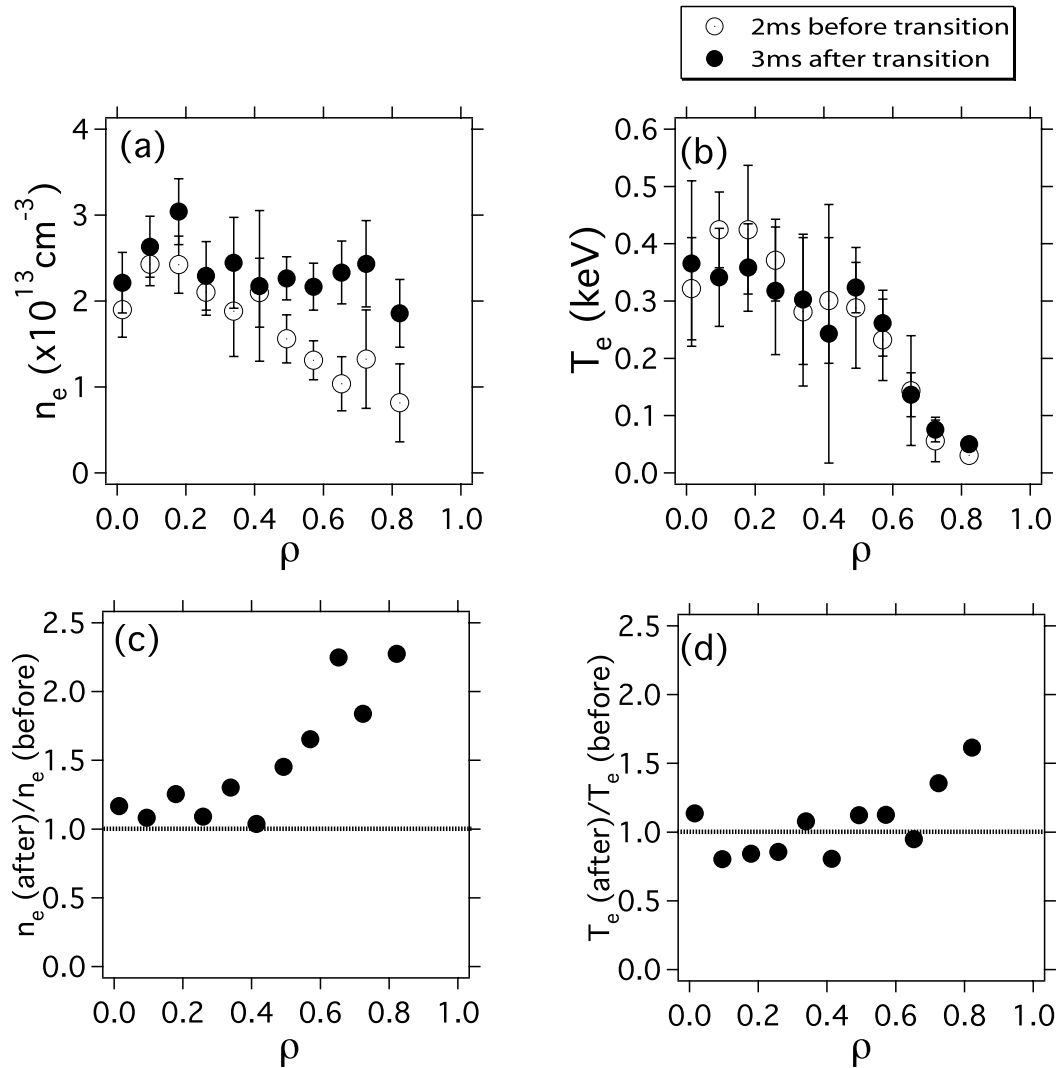


Fig. 2 (a) Electron density and (b) temperature profiles before and after L-H transition. (c) (d) Electron density and temperature profiles at the transition normalized by the values before transition, respectively.

105.3 cm) the LCFS on the L-H transition are plotted in Fig. 4, where R is a plasma major radius. The time trace of the BES signals corresponds to the local plasma density evolution. The H_α emission from the spectrometer was also plotted on the Fig. 4 using the dotted line. The H_α emission was quickly reduced with the transition time of $> 300 \mu\text{sec}$. The BES signal inside the LCFS increased, while the signal outside decreased, thereby showing good agreement with the Li beam measurement. Because the change of the BES signals was synchronized with the H_α emission, the transition of the density profile was rapid ($> 300 \mu\text{sec}$), as is the H_α reduction.

4. Existence of High Core Electron Temperature Plasma with ETB

The change of the electron temperature by the L-H transition is not clear for usual discharges, as shown in Fig. 2. However, for several specific discharges, a con-

siderable increase in the electron temperature in the core region was observed with ETB formation. Figure 5 shows electron temperature and density profiles with YAG Thomson scattering measurement for the high core electron temperature discharge 3 ms before and 2 ms after the sharp H_α signal drop. The outstanding characteristic is the core electron temperature increase after the ETB transition to approximately two times that before the transition by only NBI Heating without ECH. The achieved electron temperature of $\sim 700 \text{ eV}$ is the maximum level of the electron temperature of the CHS by two-NBI heating without ECH. The electron temperature increase is led by ETB formation.

The electron density change in the core region was very small, while the density rapidly increased by approximately 30% in the edge region ($\rho > 0.8$) after the L-H transition. These are the same characteristics as those of the other ETB plasma. The increase of the deposited NBI power was approximately 10% when the density increased from $4 \times 10^{13} \text{ cm}^{-3}$ to $5 \times 10^{13} \text{ cm}^{-3}$. On the other hand,

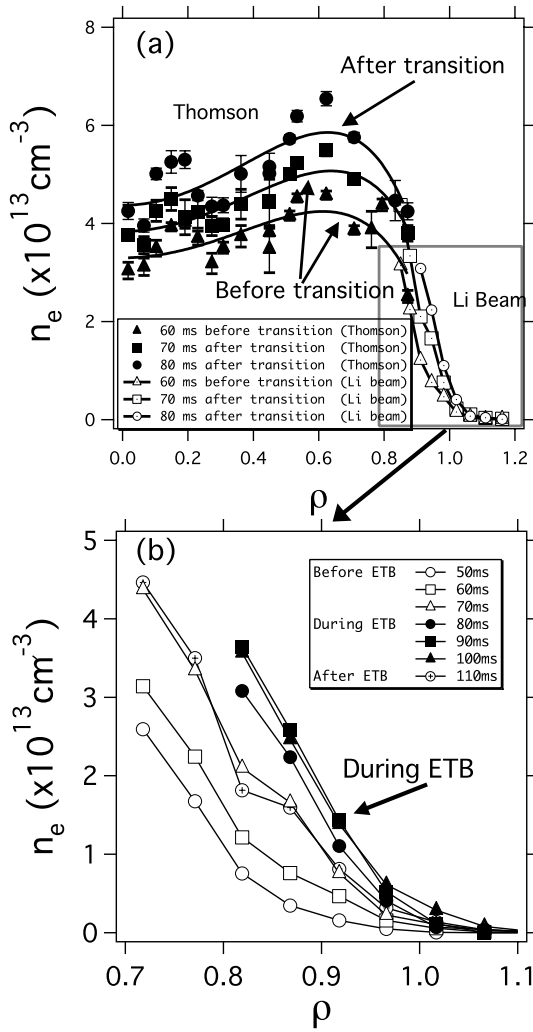


Fig. 3 (a) Density profiles comparison between YAG Thomson scattering and Li beam measurements (b) Density profiles for ETB plasmas with Li beam measurement.

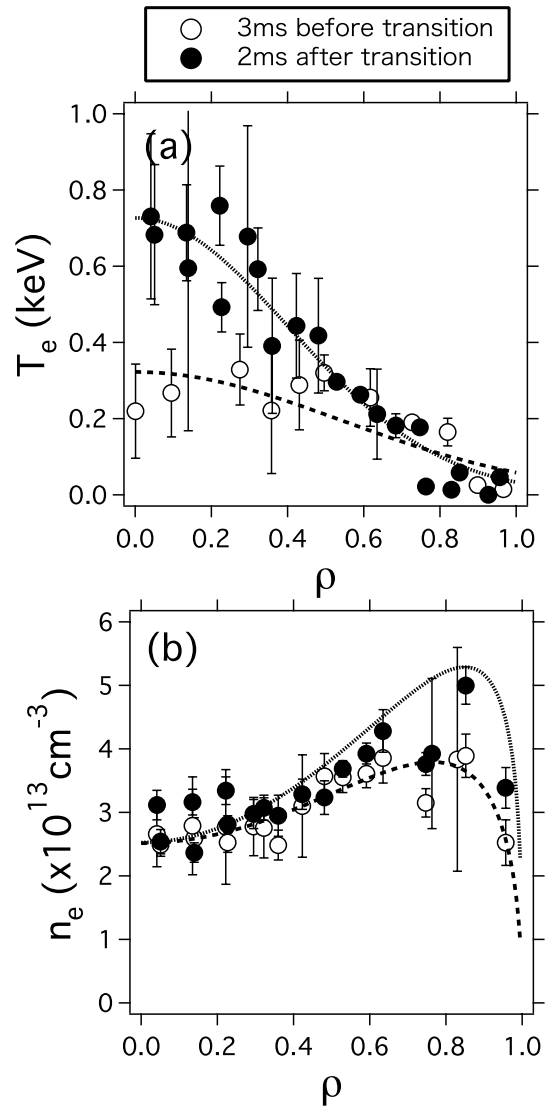


Fig. 5 Electron temperature (a) and density (b) profiles for the ETB discharge with high electron temperature in the plasma core. The open circles and the closes circles denote before and after L-H transition, respectively

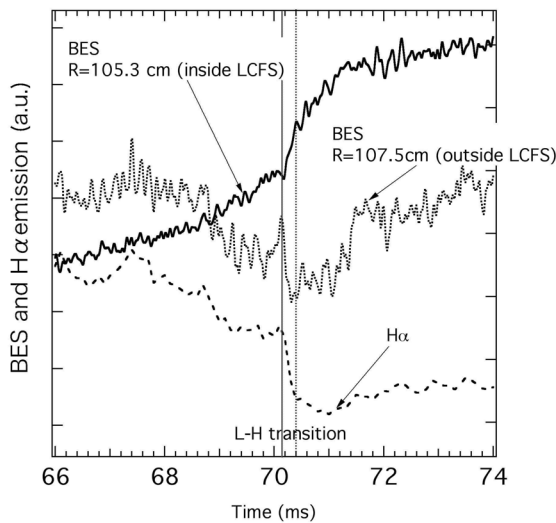


Fig. 4 Time evolution of electron density at L-H transition around LCFS with beam emission spectroscopic measurement. Dotted curve shows H_{α} signal.

there were many discharges accompanying the doubling of the edge density resulting from the ETB formation while no increase in the electron temperature was observed in the core region. Accordingly, the temperature increase cannot be explained by the deposited power increase in the peripheral plasma.

For the increase of the electron temperature, the very hollow density profile before the transition might be important. The density difference between the plasma core and edge was large ($n_e(-0.8)/n_e(0) \sim 1.6$) compared to that in the usual CHS plasma. In the typical hollow density plasma of CHS, the $n_e(-0.8)/n_e(0)$ is at most 1.2. These hollow temperature profiles are realized by gas-puffing control. Further investigation is required to confirm the relation between the hollow density profile and the electron temperature increase.

These phenomena are similar to the N-ITB resulting from the large electric field formation in the core region [3]. The N-ITB is effective at improving the energy confinement, while the ETB is effective at improving the particle confinement. This discharge might be a simultaneous achievement of the ETB and the N-ITB. However, the discharge with the high core-electron temperature was produced only by NB heating. The condition for the N-ITB formation is that the density should be below the threshold ($n_e < 0.5 \times 10^{13} \text{ cm}^{-3}$), while the density of the ETB discharge with the high electron temperature was $< 3 \times 10^{13} \text{ cm}^{-3}$. Because it is difficult to form a large electric field due to the electron root in the core region, a different physical mechanism is required for the formation of the internal transport barrier.

5. Power Threshold for ETB Formation

The NB heating power threshold for ETB formation in CHS plasmas is similar to that from the tokamak experiments. As shown in Fig. 6, the delay time of the L-H transition from the start of the second NB injection became longer as the port-through injected power decreases. When the injected power falls below ~ 1 MW, the transition time of the H_α emission becomes earlier and the back transition becomes more rapid (Fig. 6 (d)); then the H_α drop disappears altogether at the NBI injected power of 0.9 MW.

It is important to estimate the NBI power deposited into the plasma to clarify the dependence of the plasma density on the threshold power, because the plasma densities at the L-H transition depend on the injected NBI power. The deposited power is defined as follows:

$$P_{\text{deposit}} = P_{\text{port}} - P_{\text{shine}} - P_{\text{orbit}} - P_{\text{cx}}, \quad (1)$$

where the P_{deposit} is the deposited NBI Power, the P_{port} is the port-through injected power, P_{shine} is the shine-through power, and P_{orbit} and P_{cx} are the orbit loss and the charge exchange loss during the slowing-down of injected beams, respectively. We use the following formula empirically obtained in the CHS experiments for estimating the deposited power [15].

$$\frac{P_{\text{deposit}}}{P_{\text{port}}} = 1.0 - 2.35 \times 10^{-2} (R_{\text{ax}} - 0.8)^{0.509} a^{-0.061} \times \exp(-0.363 B_T) \exp(-2.6 n_e E_{\text{nbi}}^{1.35}), \quad (2)$$

where B_T (T) is the magnetic field strength at the magnetic axis, n_e ($\times 10^{14} \text{ cm}^{-3}$) is the electron density, E_{nbi} (kV) is the acceleration voltage of the NBI, R_{ax} (m) is the major radius, and a (m) is the minor radius.

Figure 7 shows the delay time of the L-H transition from the second NBI injection for three experiments. The data are plotted as a function of the deposited power normalized by the line-averaged electron density. All experiments were performed under the same condition of

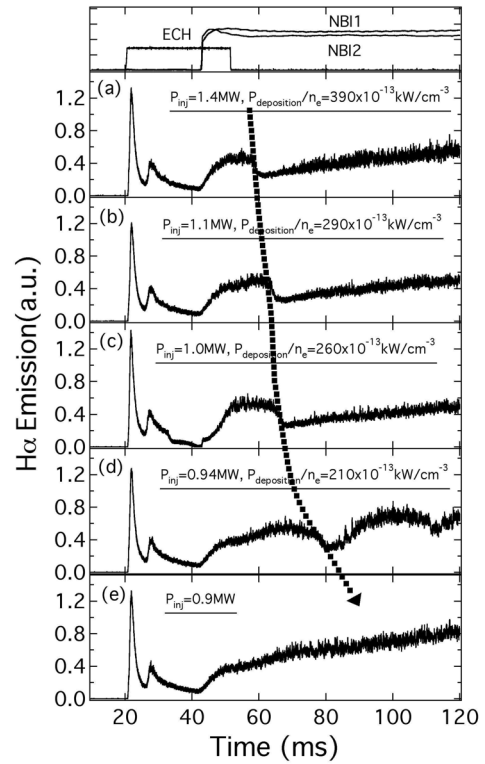


Fig. 6 H_α emissions for ETB plasmas for different NBI injected power cases. Delay time of H_α spontaneous drop after NBI injection increases with NBI power reduction. Back transition of H_α signal is quickened near the threshold power as shown in (d).

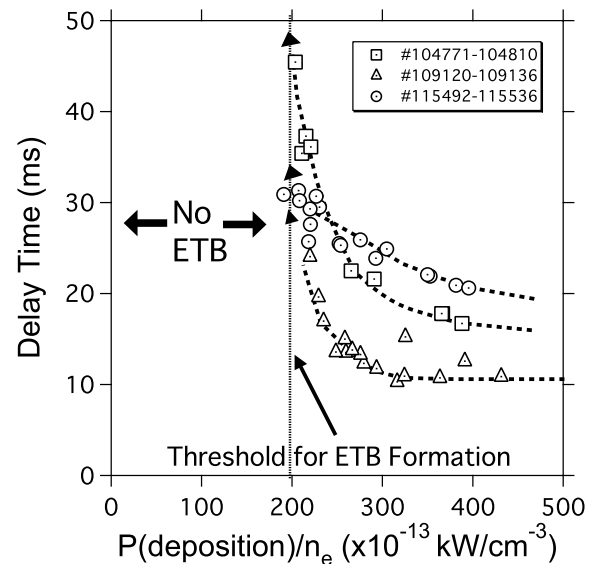


Fig. 7 Delay times of L-H transition after NBI injection are plotted as a function of deposited NBI power normalized by electron density. Circles, triangles, and squares denote data in different experiments that have different wall conditions.

$B_T = 0.95 \text{ T}$, $R_{\text{ax}} = 92.1 \text{ cm}$. As they were performed on different days, however, these data have three different wall conditions. In the case of the #115492-115536,

the timing of the second NBI injection was delayed approximately 20 ms after the first NBI injection, while in the other two cases the two NBIs were simultaneously injected. Because the wall conditions of the three experiments and the NBI injection timings varied, the delay times for the three experiments were different. However, the delay times increased when the normalized NBI power was close to the specific value of $200 \times 10^{-13} \text{ kW/cm}^{-3}$ for all the experiments, and an ETB was not formed below this specific threshold value. Accordingly, the required power for the ETB formation does not relate to the wall condition and the buildup of the discharge, which is controlled by the NBI injection timing, while the improvement of the H-factor by the ETB formation depends on the wall condition. The value of the threshold power for the barrier formation is approximately two times that expected from the tokamak H-mode scaling [16, 17]. When the delay times are plotted as a function of the NBI deposited power without being normalized, the data points are more scattered. The threshold for the formation of the ETB is determined by the deposited power per one particle; accordingly, the required NBI power for the transition increases as the density increases.

We plotted the average densities at the drop of the H_{α} emission as a function of the injected powers, as shown in Fig. 8. The ETB was formed when the deposited power exceeded the $\sim 500 \text{ kW}$ at $n_e \sim 2 \times 10^{13} \text{ cm}^{-3}$. The required power increased with increasing density, as described above. In addition, ETB formation was observed when the plasma density exceeded $\sim 1.5 \times 10^{13} \text{ cm}^{-3}$ with gas-puffing, whereas no ETB was observed when the density was below the limit. The lower density limit increased as the deposited NBI power increased. These observations for the density limit are similar to the results in the WS-

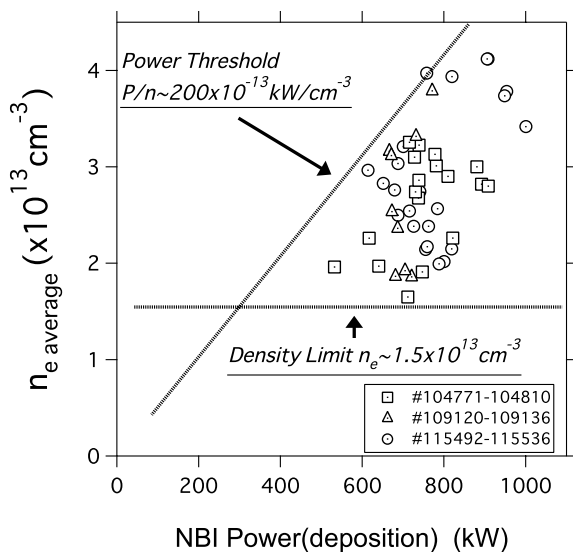


Fig. 8 Averaged electron densities for plasmas with ETB as a function of deposited NBI power.

7AS experiments [7] or the Heliotron J experiments [9].

6. Dependence of Threshold Power on Magnetic Field Configuration

The dependence of the power threshold on the magnetic field strength at the magnetic axis location of 92.1 cm was investigated for different densities and injected powers. Figure 9 shows the NBI deposited power normalized by the line-averaged density at the L-H transition as a function of the magnetic field strength. ETBs were observed from 0.83 T to 1.3 T. The plasma was not produced below $B_T = 0.83 \text{ T}$ because the inward off-axis ECH was unfavorable for producing the target plasma on the CHS. The lowest points of required power in Fig. 9 indicate the minimum required power for ETB formation. The L-H transition was not observed in the region below the dotted line, representing the lower power threshold. The same characteristic of the threshold value increasing with the field strength was observed in the tokamak experiments [18]. The ETB was not observed in $B_T > 1.3 \text{ T}$, because the plasma density increase due to the raised power in the high field range, and the necessary NBI power estimation for the ETB formation exceeded the maximum power of NBI of CHS.

The magnetic field configuration could be changed by the shift of the magnetic axis location through the control of the poloidal field coil currents in CHS. The magnetic well, the orbit of trapped particles, the plasma viscosity and the distance of the LCFS from the wall could be controlled by the magnetic axis shift. The inward shifted configuration was favorable for drift orbit optimization [19], and provided stable plasma discharge in spite of the expected instabilities from the Mercier criterion. The CHS

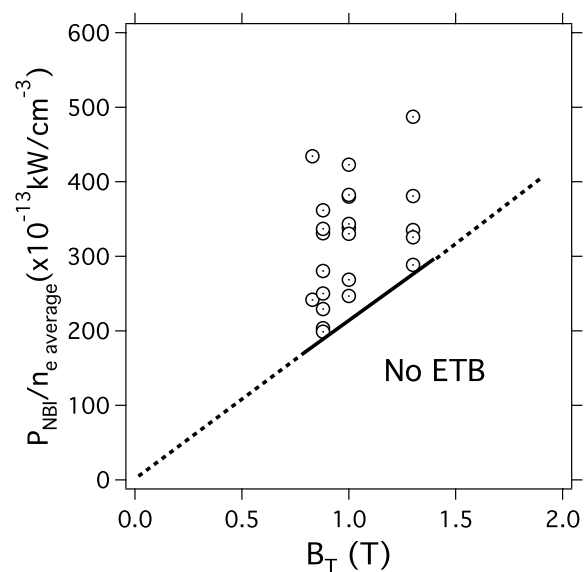


Fig. 9 NBI power normalized by density dependence on magnetic field strength at L-H transition. Line shows the power threshold for the L-H transition.

plasma came in contact with the inner wall when the magnetic axis location was less than ~ 98 cm, and the contact area increased by the inward shift. The low viscosity of the inward shift was favorable for the plasma rotation. In the N-ITB experiments, the formation of the transport barrier clearly depended on the magnetic axis location [20].

Next, the threshold power dependence on the magnetic configuration was investigated. Clear dependence of the magnetic configuration on the normalized threshold power was found, as shown in Fig. 10. The magnetic axis location of 92.1 cm is the standard configuration for realizing good plasma performance in CHS. The formation of an ETB was observed for the magnetic axis locations between 89.9 cm and 94.9 cm, as shown in Fig. 10 (a). When the magnetic axis was inside 89.9 cm or outside 94.9 cm, ETB formation was not observed. The experiments were performed for different port-through NBI powers and densities controlled by gas puffing. We did not find ETB formation below the lowest threshold value denoted by the dotted line. The threshold power shows the minimum around $R_{ax} = 93.5$ cm. The lowest power decreases as the

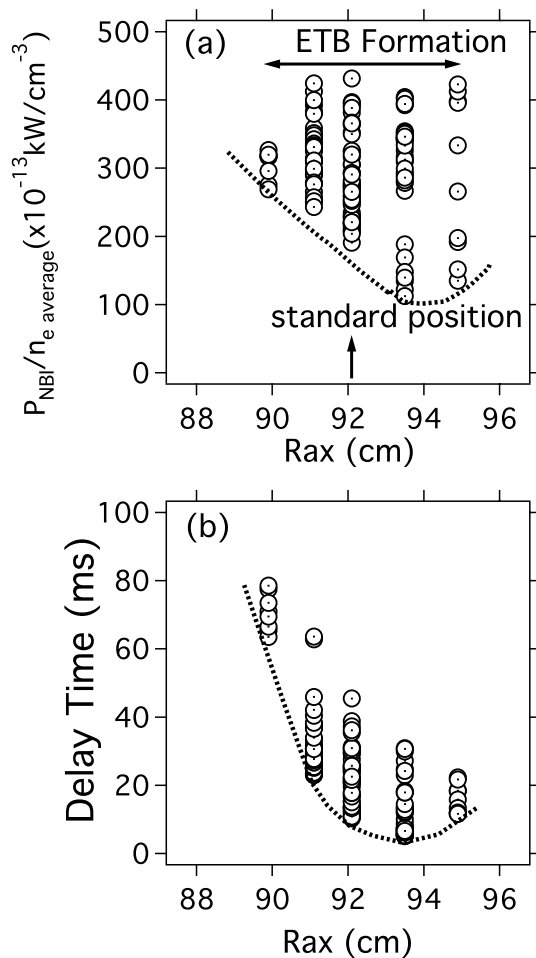


Fig. 10 At L-H transition, NBI power normalized by density (a) and delay time from the beam injection (b) dependence on various magnetic configurations (magnetic axis locations). Dotted curve denotes the power threshold.

R_{ax} increases; however, the formation of the ETB was not observed outside 94.9 cm. The same characteristic power threshold was observed for the delay time of ETB formation from the NBI injection. Figure 10 (b) shows the delay time as a function of the magnetic axis location. The delay time gets longer by the inward shift. The minimum delay time is found in the same location of 93.5 cm as the power threshold. In these experiments, whether the ETB is formed or not is judged by the observation of the transition phenomena: the observation of a spontaneous drop of H_α emissions. If the ETB is formed from the start of the NBI injection, the confirmation of the ETB formation is difficult, because of the lack of a spontaneous drop of H_α emission during the NBI injection. Because the delay time of the transition gets shorter by the outward shift, it can be hypothesized that the time of the transition coincides with the start of the NBI injection.

Consequently, the outward shift of the magnetic axis to at least $R_{ax} = 94.9$ cm is favorable for ETB formation. These results of the ETB threshold power dependence on the magnetic structure may suggest that ETB formation relates to the magnetic configuration and the plasma viscosity in the edge region, which affects the plasma rotation in the edge region. However, further investigation, for example, a detailed estimation for the magnetic structure of the ETB plasma in the edge including the plasma current, is required to obtain this conclusion. Another potential cause of the dependence is that the contact area on the inner wall is important for the barrier formation, affecting the amount of the impurities; hence, the plasma collisionality relating to the radial electric field formation by the electron root in the edge region is changed. To conclude whether the contact area is important or not, impurity measurements in the edge region are required.

7. Conclusions

An ETB similar to that in the tokamak H-mode was observed for the NB-heated plasma on CHS. The increase of the stored energy after the L-H transition indicated the improvement of the H-factor (ISS04v4) by approximately 30%. This ETB is created in the higher-density plasma than the N-ITB; accordingly, it is favorable for achieving good plasma performance.

The outstanding characteristics of the ETB formation are as follows. The spontaneous drop of the H_α signal by the L-H transition is very clear, similar to that in the tokamak experiments. The density increase with the buildup of the density gradient after the transition indicates the formation of a transport barrier at the edge region ($\rho \sim 0.9 - 1.0$). The BES measurement shows that the transition time on the density profile is very rapid ($\sim 300 \mu\text{sec}$), as is the drop of the H_α emission. A lower density limit ($1.5 \times 10^{13} \text{ cm}^{-3}$) exists for the barrier formation, similar to those in other helical plasma experiments. On the other hand, a power threshold for the barrier formation

also exists, similar to that in the tokamak H-mod experiments ($P/n \sim 200 \times 10^{-13} \text{ kW/cm}^{-3}$). The power threshold increases as the plasma density and the magnetic field strength increase; these results are similar to those of tokamak scaling. The power threshold depends on the magnetic field configuration through scanning the magnetic axis. These results are similar to those of N-ITB in CHS. Though the electron temperature change resulting from the ETB formation in the edge region is not clear, large electron-temperature increases in the core plasma were observed for several specific discharges. Investigating the mechanism of these phenomena will provide clues to spontaneously achieving high-performance plasma accompanied with internal high temperature and external high density.

- [1] A. Fujisawa *et al.*, Phys. Rev. Lett **82**, 2669 (1999).
- [2] T. Minami *et al.*, in *Proc. 26th EPS Conf. on Contr. Fusion and Plasma physics*, Maastricht (1999) p.1357.
- [3] T. Minami *et al.*, Nucl. Fusion **44**, 342 (2004).
- [4] K. Toi *et al.*, Plasma Physics and Controlled Nuclear Fusion Research (Proc. Conf. Wurzburg, 1992), IAEA, Vienna (1993) vol. 2, p.461.
- [5] K. Toi *et al.*, Plasma Phys. Control. Fusion **38**, 1289 (1996).
- [6] V. Erckmann *et al.*, Phys. Rev. Lett. **89**, 2086 (1993).
- [7] K. McCormick *et al.*, Phys. Rev. Lett. **89**, 015001 (2002).
- [8] K. Toi *et al.*, Phys. Plasmas **12**, 020701 (2005).
- [9] H. Okada *et al.*, J. Plasma Fusion Res. **80**, 883 (2004).
- [10] S. Okamura *et al.*, J. Plasma Fusion Res. **79**, 977 (2003).
- [11] S. Okamura *et al.*, Plasma Phys. Control. Fusion **46**, A113 (2004).
- [12] H. Yamada *et al.*, *Proc. of 31th EPS Conf. on Contr. on Fusion and Plasma Phys.* ECA Vol. 28G, P-5 099 (2004).
- [13] K. Nakamura *et al.*, Rev. Sci. Instrum. **76**, 013504 (2005).
- [14] T. Ohishi *et al.*, Rev. Sci. Instrum. **75**, 4118 (2004).
- [15] S. Okamura *et al.*, Nucl. Fusion **35**, 283 (1995).
- [16] J.A. Snipes *et al.*, Fusion Energy 2002 (Proc. 19th int. Conf. Lyon, 2002) CT/P-04.
- [17] T. Akiyama *et al.*, Plasma Phys. Control. Fusion *to be submitted*.
- [18] A.E. Hubbard, Plasma Phys. Control. Fusion **42**, A15 (2000).
- [19] S. Okamura *et al.*, Nucl. Fusion **39**, 1337 (1999).
- [20] T. Minami *et al.*, Plasma Phys. Control. Fusion **46**, 285 (2004).